Clays and Clay Minerals, Vol. 30, No. 5, 375–382, 1982.

THIN-FILM ANALYSIS OF CLAY PARTICLES USING ENERGY DISPERSIVE X-RAY ANALYSIS[1]

G. N. WHITE, V. E. BERKHEISER
Soil Science Department, University of Florida, Gainesville, Florida 32611

F. N. BLANCHARD
Department of Geology, University of Florida, Gainesville, Florida 32611

C. T. HALLMARK
Department of Soil and Crops Science, Texas A&M University
College Station, Texas 77843

Abstract—A standardless method of energy dispersive X-ray fluorescence in conjunction with scanning electron microscopy was used to analyze selected areas of clay-size particles of talc, pyrophyllite, and kaolinite supported by a carbon planchet. Peak intensity ratios of fluorescing elements relative to silicon were converted directly to weight or mole ratios using conversion factors determined theoretically. The conversion factors depend upon particle thickness and mass adsorption coefficients of the sample for the elements analyzed. The effects of particle thickness become significant above ~0.1 μm. Without using particle thickness corrections, the mean molar ratios of metal to Si agreed to within 6.1, 0.5, and 9.7% of the theoretical ratios for kaolinite, pyrophyllite, and talc, respectively.

Key Words—Chemical analysis, Energy dispersive X-ray analysis, Kaolinite, Particle thickness, Pyrophyllite, Scanning electron microscopy, Talc.

INTRODUCTION

With recent advances in electron optics, elemental analysis of selected areas of single clay particles has become possible by energy or wavelength dispersive X-ray analysis (EDX). Quantitative analysis is relatively easy by the "standardless" method commonly used in materials research (Philibert and Tixier, 1975; Namae, 1975; Goldstein *et al.*, 1977; König, 1976; Zaluzec, 1978, 1979). This method is restricted to flat, ultrathin samples for which corrections for fluorescence and absorption by the sample become negligibly small, and for which absolute elemental concentrations can be determined directly from X-ray intensities. Although such measurements generally require that the sample thickness be known (Colby, 1968), peak intensity ratios, rather than absolute intensities, circumvent this requirement and can be directly related to elemental ratios regardless of sample thickness as long as an "ultrathin" condition exists.

Peak intensity ratios are used because the determination of concentrations is theoretically more complex (see, for example, Colby, 1968) due to the fact that intensity is not linearly dependent on thickness and the sum of determinable elements does not, in the system studied, equal a constant. Another advantage of using ratios is that diffraction effects can cause abnormally high intensities (counting rates) without affecting peak intensity ratios (Duncomb, 1962; Hirsch *et al.*, 1962).

Factors for the conversion of peak ratios to compositions in silicates were empirically determined by Cliff and Lorimer (1975). These ratios are, however, limited to a detector matching that of the original authors. Most authors (e.g., Goldstein *et al.*, 1977; König, 1976; and Zaluzec, 1978, 1979) prefer to determine their own ratios from theoretical grounds. Such theoretical methods range from the simple (König) to the complex (Zaluzec, 1978) and vary mostly in the methods of determining the ionization cross-sections of the elements involved and in the manner in which absorption and fluorescence effects are treated.

The objectives of the present study were: (1) to apply the method of "standardless" thin film EDX to silicate minerals of known average composition, and (2) to determine the special conditions and limitations of this method for layer silicates. The method as outlined below was adapted from published work of other authors for specimens studied by transmission electron microscopy which uses higher excitation energies than scanning electron microscopy, but was tested under the conditions of the scanning electron microscope.

THEORY

In energy dispersive X-ray analysis a sample is irradiated with a beam of electrons which causes X-ray

[1] Contribution from the Agricultural Experiment Station, University of Florida, Journal Series No. 3342.

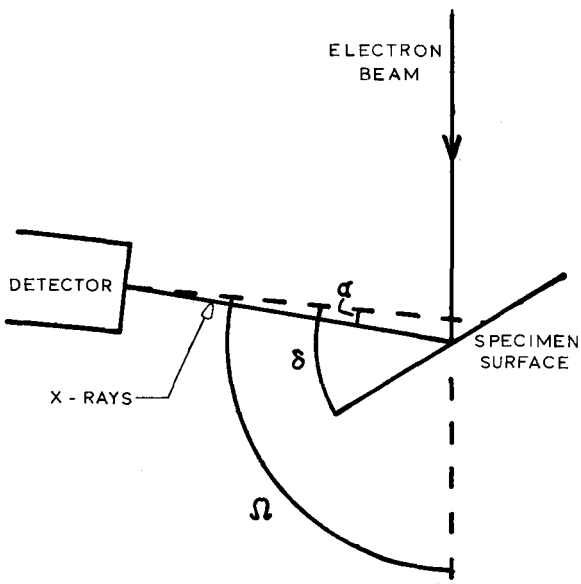

Figure 1. Schematic defining specimen geometry used in energy-dispersive X-ray analysis in the electron microscope. α = entrance angle of X-ray photons at the detector face, δ = takeoff angle (angle between detector axis and particle surface), and Ω = angle between detector axis and primary electron beam.

emission from the sample. Theoretically, the number of Kα photons ($dn_a^{K\alpha}$) produced by element A in an infinitely thin layer of thickness dt and density ρ when excited by an electron beam at energy E_0 can be determined by the relationship (after König, 1976)

$$dn_A^{K\alpha} = C_A Q_A^K (N/A_A)\omega_A^K a_A \rho \, dt \qquad (1)$$

where C_A = weight fraction of element A in the layer, Q_A^K = ionization cross-section of the K-shell for element A, ω_A^K = K-shell fluorescence yield of element A, a_A = Kα fraction of total K radiation from element A, which is equal to Kα/(Kα + Kβ), A_A = atomic weight of element A, and N = Avogadro's number.

The numerous studies of the ionization cross-sections (Q_A^K) for each element have resulted in a large number of empirical line fits to similar data (see Goldstein *et al.*, 1977, for compilation of Q_A^K equations). In our study the Bethe ionization cross-section, as quoted by König (1976), was determined from the relation

$$Q_A^K = 7.9 \times 10^{-20} [\ln(E_0/E_A^{K\ edge})]/E_0 E_A^{K\ edge}, \qquad (2)$$

where Q_A^K is the ionization cross-section in cm^2, E_0 = impact electron energy in keV, and a $E_A^{K\ edge}$ = ionization energy of the K-shell of element A in keV. Substitution of this value for Q_A^K into Eq. (1) results in

$$dn_A^{K\alpha} = 7.9 \times 10^{-20} C_A (N/A_A)\omega_A^K a_A \cdot [\ln(E_0/E_A^{K\ edge})/E_0 E_A^{K\ edge}]\rho \, dt. \qquad (3)$$

When inelastic and elastic scattering of electrons is taken into account, along with other physical factors, König (1976) showed that the integration of Eq. (1) yields

$$n_A^{K\alpha}(t) = C_A Q_A^K (N/A_A)\omega_A^K a_A h_A(\rho t), \qquad (4)$$

where $n_A^{K\alpha}(t)$ = number of Kα photons of element A produced as a function of depth, and the function

$$h_A(\rho t) = \rho t + (m/2 - \chi_A/2)(\rho t)^2 - (\chi_A m/3)(\rho t)^3, \qquad (5)$$

where m = scattering depth factor, $\chi_A = (\mu/\rho)_A/\sin\delta$, $(\mu/\rho)_A$ = mass absorption coefficient (in cm^2/g) of the specimen for X-radiation from element A, and δ = angle between specimen surface and detector axis. In the thin film approximations of $t \rightarrow 0$, h approaches 1 and thus may be neglected in most metal films (Zaluzec, 1978). However, the magnitude of this function for layer silicates must be determined.

A relationship between the number of photons as a function of depth [$n_A^K(t)$] and the corresponding measured intensity [$I_A^K(t)$] must be determined for use in quantitative analysis. König (1976) found that

$$I_A^K(t) = (6.25 \times 10^{18})[n_A^K(t)][W(E_A^K)(F/4\pi d^2)iT], \qquad (6)$$

where $W(E_A^K)$ = detector efficiency at E_A^K, F = effective area of detector, d = distance from specimen to detector, i = probe current, and T = counting time. I_A^K is expressed in counts/amp·sec.

The detector efficiency can be calculated using the relation

$$W(E_A^K) = \exp[\sum_{j=1}^{3} (\mu/\rho)_j^E \rho_j t_j/\cos\alpha], \qquad (7)$$

where j refers to each of three layers (i.e., the Si dead layer, Au coating on the detector face, and the Be window). Important angles are illustrated in Figure 1. Combining Eq. (7) with Eq. (4) gives the intensity of the K radiation of element A; but the resulting equation requires values for various instrument constants and is subject to errors resulting from fluctuation in beam current and dead time losses. If ratios of peak intensities are taken, several terms, including machine variables such as spatial angle, probe current, and counting time, are eliminated. Ratios of the peak intensities for two concentrations result by combining Eqs. (4) and (7) to obtain

$$\frac{I_A^{K\alpha}}{I_B^{K\alpha}} = \frac{C_A}{C_B} \cdot \frac{A_B \omega_A^K a_A \ln(E_0/E_A^K) E_B^K W(E_A^K) h_A}{A_A \omega_B^K a_B \ln(E_0/E_B^K) E_A^K W(E_B^K) h_B}, \qquad (8)$$

which is independent of machine factors. The right side of Eq. (8) can be factored to give

$$I_A^{K\alpha}/I_B^{K\alpha} = (C_A/C_B) k_{tfAB} (h_A/h_B), \qquad (9)$$

where

$$k_{tfAB} = \frac{A_B \omega_A^K \ln(E_0/E_A^K) E_B^K W(E_A^K) a_A}{A_A \omega_B^K \ln(E_0/E_B^K) E_A^K W(E_B^K) a_B}. \qquad (10)$$

At a given incident electron energy E_0, k_{tf} is a con-

https://doi.org/10.1346/CCMN.1982.0300508 Published online by Cambridge University Press

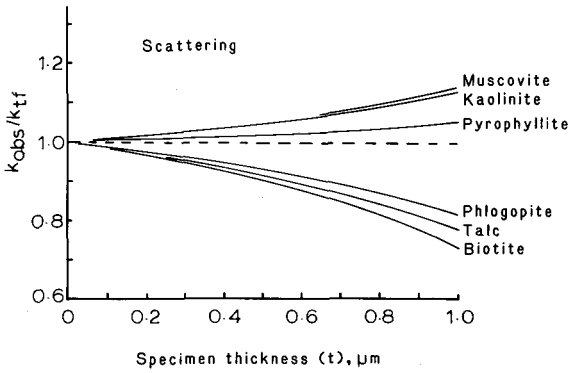

Figure 2. Calculated effects of scattering on the k_{obs}/k_{tf} ratio in selected phyllosilicates, calculated by Eqs. (5) and (11); $\delta = 30°$.

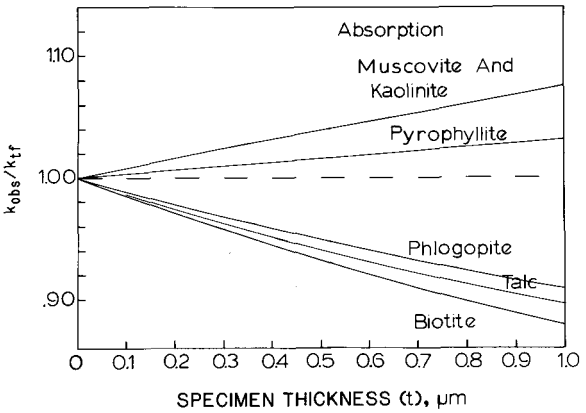

Figure 3. Calculated effects of absorption on the k_{obs}/k_{tf} ratio in selected phyllosilicates, calculated by Eq. (12); $\delta = 30°$.

stant and can be evaluated prior to analysis. The last two terms of Eq. (9) can be combined to give

$$k_{obsAB}/k_{tfAB} = h_A/h_B, \qquad (11)$$

where $k_{obsAB} = (I_A^{K\alpha}/I_B^{K\alpha})(C_B/C_A)$.

Most authors (Goldstein *et al.*, 1977; Zaluzec, 1978, 1979) ignored the scattering effect terms h_A/h_B which may lead to serious errors as illustrated in a plot of Eq. (11) as a function of thickness for several minerals (Figure 2).

Errors can also result from the other sources including absorption within the sample, absorption from the carbon coating, and various fluorescence effects. Absorption within the sample appears to be the most serious. Goldstein *et al.* (1977) stated that k_{obsAB} could be determined using the relationship

$$k_{obsAB} = k_{tfAB}[(\mu/\rho)_B/(\mu/\rho)_A] \cdot \frac{1 - \exp[-(\mu/\rho)_A(\csc\delta)\rho t]}{1 - \exp[-(\mu/\rho)_B(\csc\delta)\rho t]}, \qquad (12)$$

where $(\mu/\rho)_A$ = mass absorption coefficient of the specimen for X-radiation from element A, ρ = specimen density, and t = the specimen thickness. The effect of specimen thickness on the absorption correction (in terms of the ratio k_{obsAB}/k_{tfAB}) is shown in Figure 3 where A and B represent Al and Si, respectively. The correction is almost linear in the thickness range studied wherein the slope was determined mostly by the ratio of the mass absorption coefficients.

Philibert and Tixier (1975) found that fluorescence from thin foils resulted from two sources, the continuum and the characteristic lines of the sample. The fluorescence correction is generally small and is considered negligible for films with $(\mu/\rho)\rho t < 0.1$ (Philibert and Tixier, 1975; Zaluzec, 1978).

The total effect of thickness on k_{obs} can be determined by combining Eqs. (6), (12), and (13) to form the equation

$$k_{obs} = k_{tf}\frac{[1 + (m/2 - \chi_A/2)\rho t - (\chi_A m/3)(\rho t)^2]}{[1 + (m/2 - \chi_B/2)\rho t - (\chi_B m/3)(\rho t)^2]} \cdot \frac{(\mu/\rho)_B}{(\mu/\rho)_A}\frac{\{1 - \exp[(\mu/\rho)_A\rho t(\csc\delta)]\}}{\{1 - \exp[(\mu/\rho)_B\rho t(\csc\delta)]\}}. \qquad (13)$$

This equation is shown graphically in Figure 4 for various minerals. Comparison of Figures 2 and 3 with Figure 4 shows that the scattering effects are of nearly the same magnitude as absorption effects.

Beam spreading must also be considered in selected area analysis (Goldstein *et al.*, 1977). As the electron beam of energy E_0 passes through the particle, scattering by the sample causes an increase in the beam radius according to the relationship

$$b = 6.25 \times 10^5(\bar{Z}/E_0)(\rho/A)^{1/2}t^{3/2}, \qquad (14)$$

where b is the additional beam radius (in cm) at a thickness t (in cm) in a film of material with density ρ, average atomic number $\bar{Z}$, and average atomic weight A. Although the elemental analysis by the ratio method does not change with dimensions of the beam, beam spreading imposes a minimum dimension on the size of particles which can be analyzed (Figure 5), depending on their thicknesses. For ultrathin samples beam spreading is negligible.

MATERIALS AND METHODS

Three minerals were used to test the usefulness of the theory outlined above. Well-crystallized kaolinite (KGa-1) from the Clay Minerals Repository of The Clay Minerals Society was used as received. Talc (Fowler, New York) and pyrophyllite (Hillsborough, North Carolina) were purchased from Ward's Natural Science Establishment, Rochester, New York. These minerals were selected because they are presumably compositionally pure and homogeneous (no minor elements were detectable by EDX). The talc specimen appeared to be homogeneous and was broken into smaller frag-

https://doi.org/10.1346/CCMN.1982.0300508 Published online by Cambridge University Press

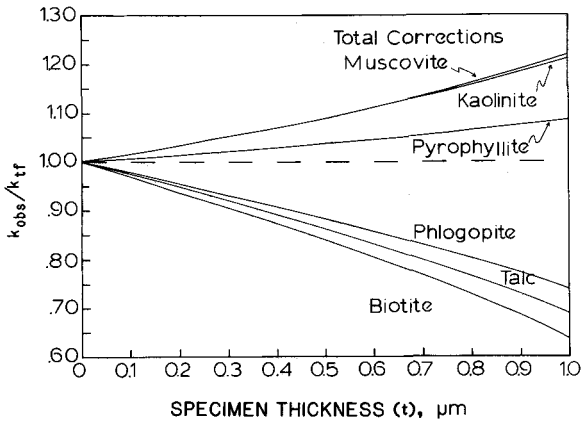

Figure 4. Calculated effects of scattering and absorption on the k_{obs}/k_{tf} ratio in selected phyllosilicates, calculated by Eq. (13); $\delta = 30°$.

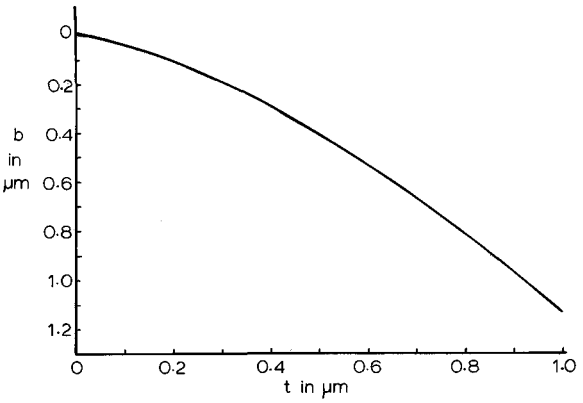

Figure 5. Calculated effects of beam broadening on beam radius for a specimen of pyrophyllite, $\rho = 2.90$, $E_0 = 20$ kv.

ments followed by comminution in deionized water for 30 min. Pyrophyllite crystals were separated from the iron oxide-containing matrix and subsequently comminuted in deionized water for 30 min. After comminution, talc and pyrophyllite were oven dried and stored for use. Each mineral was saturated with Ba using barium acetate solution adjusted to pH 5.0, for a determination of its cation-exchange capacity and EDX analysis. X-ray diffraction data of powdered specimens of the talc and pyrophyllite were obtained on a Diano XRD700 X-ray diffractometer using CuKα X-radiation and a graphite crystal monochromator at a scan rate of 0.4°2θ/min.

Dispersed suspensions were dried from highly dilute suspensions (to prevent particle overlap) onto carbon planchets under a high intensity light source and subsequently coated with carbon for scanning electron microscopy (SEM) (see Berkheiser and Monsees, 1982). All observations were made at 20 kV with a spectrum acquisition clock time of 10–30 sec. The SEM used was a Hitachi S450 with a Kevex 7000 μX analyzer, a 20-eV channel width, and a 10-keV range. The detector characteristics as stated by the manufacturer were: Be window thickness = 0.008 mm, Au coating thickness = 0.05 μm, Si dead layer thickness = 1 μm, resolution of 155 eV at 5.9 keV at 1000 counts per second, and detector area = 30 mm^2.

Peak ratios used in this study were obtained as ratios of the channels of the peak centroid for the elements found in each mineral. Better counting statistics result through the use of windows, an analytical feature of most EDX units, but windows were not used due to peak deconvolution problems. Fluorescence from the continuum of X-rays and backscattered electrons from the graphite stub was assumed to be negligible as a first approximation. The geometry of the electron microscope and the EDX detector is shown in Figure 1 with the important angles labelled.

Background intensity at each peak centroid (channel with the highest number of counts in the peak of a single element) produced by the continuum originating in the graphite support and in the specimen was calculated by the relation:

$$I = R(E_0 - E)/E, \qquad (14)$$

where I is the calculated intensity at energy E, E_0 is the energy of the primary electron beam, and R is constant (Reed, 1975). Eq. (14) was fitted to mineral spectra between 2.00 and 4.00 keV in order to obtain a value for R for a particular specimen. The observed intensity of each peak centroid (1.26 keV for Mg, 1.50 keV for Al, and 1.74 keV for Si) was adjusted by the calculated intensity of the background.

Overlap of the peak of one element on the centroid of a neighboring element was determined empirically from spectra of separate samples of $Mg(OH)_2$, quartz, and $Al(OH)_3$. Table 1 gives the results after each centroid channel of the single-metal oxide and hydroxide was corrected for background.

RESULTS AND DISCUSSION

Results of X-ray powder diffraction analysis of the talc and pyrophyllite specimens are given in Table 2 with hkl assignments from Stemple and Brindley (1960)

Table 1. Peak overlap of one element peak on the centroid channel of the peaks of neighboring elements.

Peak originating from	Percent overlap on the centroid of[1]		
	Mg	Al	Si
Mg	—	1.4	0.0
Al	3.0	—	7.5
Si	0.0	6.6	—

[1] For example, number of counts in Mg centroid would be reduced by 3.0% of the Al centroid because of peak overlap from Al; or Mg counts = observed Mg counts − 0.030 (Al centroid counts).

https://doi.org/10.1346/CCMN.1982.0300508 Published online by Cambridge University Press

Table 2. Observed X-ray diffraction data for powder samples of talc and pyrophyllite.

Talc[1]			Pyrophyllite[2]		
d (Å)	I	hkl	d (Å)	I	hkl
17.6 (S)	2	—	9.30	25	001
9.30	80	002	4.60	10	002
5.90 (S)	2	—			020
4.67	50	004	4.44	11	110
3.12	100	006			021
2.63	1	$20\bar{2}$	4.25 (Q)	50	
2.60	2	$13\bar{2}$			$11\bar{2}$
2.47	3	132	4.17	40	111
		$20\bar{4}$			022
2.34	6	008	3.34 (Q)	100	
2.21	1	$13\bar{4}$	3.08	25	006
2.10	1	$13\bar{6}$			130
1.87	30	00·10			$20\bar{2}$
1.67	2	$24\bar{4}$	2.57–2.53	12	200
		138			$13\bar{2}$
1.56	7	00·12			026
1.53	2	060	2.45 (Q)	20	
		$33\bar{2}$	2.42	20	132
					$20\bar{4}$
			2.28 (Q)	15	
			2.24 (Q)	10	
			2.12 (Q)	12	
			1.98 (Q)	12	
			1.82 (Q)	30	
			1.67 (Q)	12	
			1.66 (Q)	5	
			1.54 (Q)	23	
			1.49	10	060
					$33\bar{2}$
			1.45 (Q)	2	

[1] Matched with data of Stemple and Brindley (1960). S = smectite impurity.

[2] Matched with data of Brindley and Wardle (1970) for monoclinic pyrophyllite. Q = quartz.

for talc and Brindley and Wardle (1970) for pyrophyllite. The talc specimen contained a small amount of a higher-spacing mineral which was presumably smectite. The pyrophyllite specimen contained a large quantity of quartz. However, the EDX of single particles was not affected by the presence of quartz because pyrophyllite was readily identified by its Al content. Data for the 060 reflections (1.53 Å for talc, 1.49 Å for pyrophyllite) further substantiate the identity of the layer silicate components of the specimens.

Values calculated for k_{tf} using Eq. (10) at an E_0 = 20 keV and with element B = Si are shown in Table 3. These values were calculated using the fluorescence yield values, ω^K, of Colby (1968); the Kα contribution to total K radiation was determined from the Kβ/Kα values of Slivinsky and Ebert (1972) and McCrary *et al.* (1971). The values of a_A (fraction of Kα in total K radiation) for Mg, Al, and Si were assumed to be 1 because the Kα and Kβ peaks of these elements were not resolved by the detector. For elements with atomic number greater than 14, corrections are needed (Reed,

Table 3. Calculated values for k_{tf} at E_0 = 20 kV, α = 0.

Element	k_{tf}
Na	0.3277
Mg	0.5980
Al	0.7861
Si	1.0000
K	0.7808
Ca	0.8184
Ti	0.7561
V	0.7182
Cr	0.6965
Mn	0.6476
Fe	0.6107
Co	0.5507
Ni	0.5183
Cu	0.4440
Zn	0.3954

1975). The values for detector efficiency were determined from Eq. (9) using Heinrich's values for mass absorption coefficients and using detector film thicknesses obtained from the manufacturer. The value for detector efficiency shown in Table 4 are much lower than the values which were obtained by extrapolation of the graph shown in the owner's manual but gave much better results when used in the analyses. The values used for α = 0 were consistent with the earlier graphs of absorption and scattering effects.

The calculated k_{tf} values for elements typically found in soil minerals (Table 3) were less than one and became progressively smaller as Z deviated in either direction from that of Si. For Na, Mg, and Al ($Z < 14$) the calculated k_{tf} were less than 1 because all of the factors in the equation except ln (E_0/E_A^K) were smaller for those elements than for Si. For the elements with $Z > 14$, the

Table 4. Values calculated for $W(E^{K\alpha})$ using the detector constants obtained from the manufacturer.

	Efficiency (%)		
	Incident angle, α		
Element	0°	15°	30°
Na	24.14	22.96	19.37
Mg	41.51	40.24	36.23
Al	56.72	55.60	51.96
Si	68.41	67.50	64.50
K	69.65	68.77	65.86
Ca	74.71	73.95	71.42
Ti	84.34	83.83	82.15
V	87.59	87.19	85.82
Cr	90.10	89.77	88.65
Mn	92.04	91.78	90.87
Fe	93.57	93.35	92.61
Co	94.75	94.57	93.95
Ni	95.70	95.55	95.05
Cu	96.45	96.33	95.92
Zn	97.06	96.96	96.61

https://doi.org/10.1346/CCMN.1982.0300508 Published online by Cambridge University Press

Table 5. Observed peak intensities, peak intensity ratios, and mole ratios for talc obtained by single particle analysis using standardless EDX.

Particle number	Peak intensity[1] counts		Peak intensity ratio	Mole ratio[2,3]
	Mg	Si	Mg/Si	Mg/Si
1	1268	2874	0.4412	0.6622
2	253	532	0.4756	0.7138
3	928	2018	0.4599	0.6902
4	513	1053	0.4871	0.7310
5	786	1709	0.4598	0.6901
6	622	1558	0.3992	0.5991
7	908	2097	0.4329	0.6497
8	612	1430	0.4281	0.6425
Mean	—	—	0.4480	0.6723
Std. dev.	—	—	0.0283	0.0425
CV(%)			6.3	6.3

[1] For the peak centroids of Mg (1.25 keV) and Si (1.74 keV) on the spectrum analyzer. Intensities have been corrected for background continuum according to Eq. (15), and for peak overlap.
[2] Theoretical ratio is 0.75.
[3] Calculated using Eqs. (9) and (10) with no correction for thickness.

values for atomic weight and E_A^K are higher than for Si, and $\ln(E_0/E_A^K)$ is lower than for Si resulting in a k_{tf} of less than 1.

The results of the analysis of single particles of talc are given in Table 5 and those for pyrophyllite and kaolinite in Table 6. The coefficient of variation for peak intensity ratios and molar ratios for talc, pyrophyllite, and kaolinite were 6.3, 2.8, and 0.1%, respectively. Several factors such as counting statistics of the detector, particle thickness, microscopic composition and takeoff angle may contribute to the variability. Other instrumental factors such as probe current variations, counting time, and dead time cancel out according to Eq. (9). The standard deviation in total counts for a given channel in usually given as $2\sqrt{N}$, where N is the number of counts in the channel (Goldstein and Colby, 1975). To achieve a 2% deviation in N, at least 10^4 counts must be obtained. The deviation in individual observed peak intensities thus ranges from 31% (talc particle number 2, Mg peak) to 3.3% (pyrophyllite particle number 3, Si peak). Counting statistics likely contribute significantly to the variability in the peak intensity ratios. Differences in particle thickness and composition (or mass absorption coefficient) as well as takeoff angle also contribute to the variability in intensity ratios in the manner described by Eq. (13). For example, the takeoff angle may be affected by the surface morphology of a particle as a result of shrinkage during specimen preparation, etching of crystal (or particle) faces, as well as the intrinsic shape of the particle. At a "measured" takeoff angle of 30° and with ±10° variability in surface morphology, k_{obs}/k_{tf} for a kaolinite particle 0.1 μm thick ranges from 1.025 at a 20° "actual" takeoff angle to 1.012 at a 40° "actual" takeoff angle. A 10° variability in "actual" takeoff angle of thicker particles produces even more variability in k_{obs}/k_{tf}. Minimizing the effects of these parameters will be discussed in a subsequent paper.

The Al/Si mole ratio obtained for pyrophyllite (Table 6) comes very close to the theoretical values even without the thickness corrections shown in Figure 4. Talc (Table 5) and kaolinite (Table 6), however, apparently need thickness corrections to bring the metal/Si ratio

Table 6. Observed peak intensities, peak intensity ratios, and mole ratios for pyrophyllite and kaolinite obtained by single particle standardless EDX.

Minerals	Particle number	Peak intensity[1] counts		Peak intensity ratio	Mole ratio[2,3]
		Al	Si	Al/Si	Al/Si
Pyrophyllite	1	1322	3385	0.3905	0.4772
	2	1031	2413	0.4273	0.5222
	3	1556	3766	0.4132	0.5050
	4	824	2055	0.4010	0.4901
	5	654	1542	0.4242	0.5184
	Mean	—	—	0.4122	0.5026
	Std. dev.	—	—	0.0115	0.0190
	CV (%)			2.79	3.78
Kaolinite	1	340	392	0.8672	1.0599
	2	376	433	0.8688	1.0618
	Mean	—	—	0.8680	1.0609
	Std. dev.	—	—	0.0011	0.0013
	CV (%)			0.13	0.12

[1] For peak centroids of Al (1.50 keV) and Si (1.74 keV) on the spectrum analyzer. Intensities have been corrected for background continuum according to Eq. (15), and for peak overlap.
[2] Theoretical ratios are: kaolinite, 1.00; pyrophyllite, 0.50.
[3] Calculated using Eqs. (9) and (10) with no corrections for thickness.

closer to theoretical values. At 0.1 μm thickness, the correction (k_{obs}/k_{tf}) is 0.97 for talc (Figure 6) and 1.02 for kaolinite (Figure 4) and would be even larger for thicker particles. The values shown in Table 6 are within the range calculated for particles less than 1.0 μm thick for the three minerals observed. Thus, without measurements of particle thicknesses, the standardless method of analysis gives reasonable results, although measurement of particle thickness would provide more accurate k_{obs}/k_{tf}. Further improvement in particle orientation on the support planchet (Berkheiser and Monsees, 1982), optimization of total spectrum acquisition time, and proper adjustment of the takeoff angle will likely reduce errors involved in measurements of this type.

ACKNOWLEDGMENTS

The authors express their gratitude to Drs. H. C. Aldrich and G. W. Erdos for their assistance in the use of the electron microscope. This work was supported in part by a Low Energy Technology Grant from the Institute of Food and Agricultural Sciences.

REFERENCES

Berkheiser, V. E. and Monsees, M. B. (1982) Dispersion of clays on graphite supports for X-ray microprobe analysis: *Soil Sci. Soc. Amer. J.* **46** (in press).

Brindley, G. W. and Wardle, R. (1970) Monoclinic and triclinic forms of pyrophyllite and pyrophyllite anhydride: *Amer. Mineral.* **55,** 1259–1272.

Cliff, G. and Lorimer, G. W. (1975) The quantitative analysis of thin specimens: *J. Microsc.* **103,** 203–207.

Colby, J. W. (1968) Quantitative microprobe analysis of thin insulating films: *Adv. X-Ray Anal.* **11,** 287–305.

Duncomb, P. (1962) Enhanced X-ray emission from extinction contours in a single-crystal gold film: *Phil. Mag.* **7,** 2101–2105.

Goldstein, J. I. and Colby, J. W. (1975) Special techniques in the X-ray analysis of samples: in *Practical Scanning Electron Microscopy,* J. I. Goldstein and H. Yakowitz, eds., Plenum Press, New York, 435–490.

Goldstein, J. I., Costley, J. L., Lorimer, G. W., and Reed, S. J. B. (1977) Quantitative X-ray analysis in the electron microscope: *SEM 1977* **1,** 315–325.

Hirsch, P. B., Howie, A., and Whelan, M. J. (1962) On the production of X-rays in thin metal films: *Phil. Mag.* **7,** 1095–2100.

König, R. (1976) Quantitative X-ray microanalysis of thin foils: in *Electron Microscopy in Mineralogy,* H. R. Wenk, ed., Springer-Verlag, New York, 526–536.

McCrary, H. J., Singman, L. V., Ziegler, L. H., Looney, L. D., Edmonds, C. M., and Harris, E. (1971) K-fluorescent X-ray relative intensity measurements: *Phys. Rev.* **A4,** 1745–1750.

Namae, Takao (1975) A method for quantitative analysis for thin specimens by energy dispersive spectrometer fitted to transmission electron microscope: *J. Electron Microsc.* **24,** 1–6.

Philibert, J. and Tixier, R. (1975) Electron probe microanalysis of transmission electron microscope specimens: in *Physical Aspects of Electron Microscopy and Microbeam Analysis,* B. Siegel and D. R. Beaman, eds., Wiley, New York, 333–354.

Reed, S. J. B. (1975) *Electron Microprobe Analysis:* Cambridge University Press, New York, 308–310.

Slivinsky, V. W. and Ebert, P. J. (1972) Kβ/Kα X-ray transition-probability ratios for elements $18 \leq Z \leq 39$: *Phys. Rev.* **A5,** 1581–1586.

Stemple, I. S. and Brindley, G. W. (1960) Structural study of talc and talc-tremolite relations: *J. Amer. Ceram. Soc.* **43,** 34–42.

Zaluzec, N. J. (1978) An analytical electron microscope study of the omega phase transformation in a zirconium-niobium alloy: *Oak Ridge National Laboratory Report ORNL/TM6705,* National Technical Information Service, Springfield, Virginia, 31–141 pp.

Zaluzec, N. J. (1979) Quantitative X-ray microanalysis: Instrumental considerations and applications to materials science: in *Introduction to Analytical Electron Microscopy,* J. J. Hren, J. I. Goldstein, and D. C. Joy, eds., Plenum Publishing Corp., New York, 121–167.

(Received 15 December 1980; accepted 15 December 1981)

Резюме—Использовался бесстандартный метод энергетическо-дисперсионной рентгеновской флуоресценции вместе сосканирующей электронной микроскопией для химического анализа выбранных мест частиц талька, пирофиллита, и каолинита о размере частиц глины, поддерживаемых угольной основой. Соотношения максимальной интенсивности флуоризуюших элементов по отношению к кремнию были превращены непосредственно в весовые или молярные соотношения, используя теоретически определенные факторы. Эти факторы зависят от толщины частиц и коэффициентов массовой адсорбции образца для анализированных элементов. Эффекты толщины частиц становятся значительными выше ~0,1 μм. Средние молярные соотношения металла к Si, без использования поправок на толщину частиц, согласовались с теоретическими соотношениями в пределах 6,1, 0,5, и 9,7% для каолинита, пирофиллита и талька, соответственно. [E.C.]

Resümee—Eine standardfreie Methode der energiedispersiven Röntgenfluoreszenz in Verbindung mit Rasterelektronenmikroskopie wurde verwendet, um ausgewählte Bereiche von Talk, Pyrophyllit, und Kaolinit in der Größe der Tonfraktion chemisch zu untersuchen, die auf Kohlenstoffträgern aufgebracht waren. Die Peakintensitätsverhältnisse der fluoreszierenden Elemente im Vergleich zu Silizium wurden direkt in Gewichts- oder Molverhältnisse umgerechnet, wozu theoretisch bestimmte Umrechnungsfaktoren verwendet wurden. Die Umrechnungsfaktoren hängen von der Teilchengröße und von den Masseadsorptionskoeffizienten der Probe für die analysierten Elemente ab. Die Auswirkungen der Teilchendicke wurde über etwa 0,1 μm von Bedeutung. Ohne Korrektur der Teilchendicke weicht das durchschnittliche Molverhältnis Metall/Si für Kaolinit, Pyrophyllit bzw. Talk um etwa 6,1%, 0,5% bzw. 9,7% von den theoretischen Verhältnissen ab. [U.W.]

Résumé—Une méthode sans standard de fluorescence de rayons-X dispersant l'énergie en conjonction avec la microscopie balayante à électrons a été utilisée pour analyser chimiquement des régions choisies de particules de talc, de pyrophyllite, et de kaolinite de taille de l'argile. Les plus hautes proportions d'intensité d'éléments fluorescents relativement à la silice ont été convertis directement en proportions de poids, ou molaires en utilisant des facteurs de conversions determinés théoriquement. Les facteurs de conversion dépendent de l'épaisseur et des coéfficients d'adsorption de masse de l'échantillon pour les éléments analysés. Les effets de l'épaisseur de la particule devenaient significatifs au dessus d'~0,1 μm. Sans utiliser les corrections pour l'épaisseur de particule, les proportions molaires moyennes du métal à la silice s'accordaient à 6,1, 0,5, et 9,7% près avec les proportions théoriques pour la kaolinite, la pyrophyllite, et le talc, respectivement. [D.J.]

https://doi.org/10.1346/CCMN.1982.0300508 Published online by Cambridge University Press